VIP Biosensors Very Important Paper

How to cite: *Angew. Chem. Int. Ed.* **2022**, *61*, e202204252
International Edition: doi.org/10.1002/anie.202204252
German Edition: doi.org/10.1002/ange.202204252

A DNA Barcode-Based Aptasensor Enables Rapid Testing of Porcine Epidemic Diarrhea Viruses in Swine Saliva Using Electrochemical Readout

Amanda Victorious[+], Zijie Zhang[+], Dingran Chang, Roderick Maclachlan, Richa Pandey, Jianrun Xia, Jimmy Gu, Todd Hoare, Leyla Soleymani, and Yingfu Li**

Abstract: Pen-side testing of farm animals for infectious diseases is critical for preventing transmission in herds and providing timely intervention. However, most existing pathogen tests have to be conducted in centralized labs with sample-to-result times of 2–4 days. Herein we introduce a test that uses a dual-electrode electrochemical chip (DEE-Chip) and a barcode-releasing electroactive aptamer for rapid on-farm detection of porcine epidemic diarrhea viruses (PEDv). The sensor exploits inter-electrode spacing reduction and active field mediated transport to accelerate barcode movement from electroactive aptamers to the detection electrode, thus expediting assay operation. The test yielded a clinically relevant limit-of-detection of 6 nM (0.37 $\mu g\,mL^{-1}$) in saliva-spiked PEDv samples. Clinical evaluation of this biosensor with 12 porcine saliva samples demonstrated a diagnostic sensitivity of 83 % and specificity of 100 % with a concordance value of 92 % at an analysis time of one hour.

Introduction

It is widely disseminated that human, animal, and environmental health is tightly interconnected. Pathogens such as coronaviruses (CoVs) cause severe respiratory, enteric, and systemic infections in human and animal hosts,[1,2] jeopardize animal husbandry and food supply,[3] and have potentially devastating environmental and global biodiversity consequences.[4] Furthermore, viral outbreaks in livestock pose continuous threats to human health, carrying risks of human zoonotic infections or the emergence of transboundary viral strains with pandemic potential, as evidenced by the recent COVID-19 pandemic.[5] In fact, more than 70 % of all emerging infections are believed to have animal origins.[6] Additionally, infectious animal diseases pose a clear economic threat, affecting local food production, national economies, and global trade. In 2013, the introduction of porcine epidemic diarrhea virus (PEDv)—an emerging and highly transmittable CoV—devastated 10 % of the US commercial swine population in 31 states within a span of 18 months, leading to economic losses of > US $400 million.[2]

Although biosecurity measures in the commercial swine industry is comprehensive in many countries including Canada and United States, the rapid and recurrent spread of PEDv demonstrates the vulnerability of the farming industry to emerging pathogens. The current biosecurity surveillance measures for animal diseases such as PEDv rely on polymerase chain reaction (PCR) testing, which requires analysis at centralized laboratory, specialized equipment and technical expertise, and transport and turnaround times between sample submission and diagnosis spanning 2–4 days.[7] The lack of rapid and on-farm testing allows emerging animal pathogens to spread, increasing morbidity and mortality rates in animals.[8] Immunoassays are popular alternatives to PCR for PEDv detection, which reduce sample-to-result time and assay complexity by eliminating the need for reverse transcription and target amplification. These assays rely on the use of antibodies as bio-recognition elements and are often integrated into engineered detection platforms or devices for rapid testing such as lateral flow assays (LFAs),[9–11] enzyme-linked immunosorbent assays (ELISA),[12–17] and electrochemical assays.[18–20] Although rapid, these methods, all based on antibody-based sandwich assays, either require multi-step processing such as washing, labeling, or addition of reagents (ELISA and electrochemical assays) or suffer from low clinical sensitivity and specificity partly stemming from the poor stability and cross-reactivity of the antibodies (LFAs).[7]

[*] A. Victorious,[+] Dr. R. Pandey, Prof. Dr. T. Hoare, Prof. Dr. L. Soleymani, Prof. Dr. Y. Li
School of Biomedical Engineering, McMaster University
1280 Main Street West, Hamilton, Ontario, L8S 4K1 (Canada)
E-mail: soleyml@mcmaster.ca
liying@mcmaster.ca

Dr. Z. Zhang,[+] Dr. D. Chang, J. Xia, J. Gu, Prof. Dr. Y. Li
Department of Biochemistry and Biomedical Sciences,
McMaster University (Canada)

R. Maclachlan, Prof. Dr. L. Soleymani
Department of Engineering Physics,
McMaster University (Canada)

Prof. Dr. T. Hoare
Department of Chemical Engineering,
McMaster University (Canada)

Prof. Dr. L. Soleymani, Prof. Dr. Y. Li
Michael G. DeGroote Institute for Infectious Disease Research,
McMaster University (Canada)

[+] These authors contributed equally to this work.

DNA aptamers, a class of functional nucleic acids selected in vitro for specific target binding, offer several key advantages over antibodies for the development of rapid tests such as their small size, high chemical and thermal stability, easy and precise modification, compatibility with DNA machines and consequently reagent-less sensing, scalable production and minimal batch-to-batch variation.[21] In addition, it has been shown that aptamers can be used to directly detect targets present in clinical samples,[22,23] making these molecular recognition elements increasingly important for developing rapid diagnostic devices. In the past few decades, many important DNA aptamers have been selected for rapid diagnosis of viral diseases including human immunodeficiency virus (HIV), influenza, porcine reproductive and respiratory syndrome virus (PRRSv), African swine fever virus (ASFv) and coronaviruses like SARS-CoV[24–26] and MERS.[27] However, there are no aptamers currently available for detecting PEDv.

We sought to develop a reagent-less electrochemical aptamer-based sensor for rapid PEDv sensing to combine the advantages of aptamers with the ultra-sensitivity of electrochemical readout. The existing aptamer-based electrochemical sensors typically employ target-induced structure switching.[28–30] The integration of the redox label directly on the structure-switching aptamer that is immobilized on the sensing electrode often results in large background signals even before target capture due to the reversibility of the system[28] and/or the flexibility of the DNA aptamer.[31–33] Aptamers relying on the displacement of a labeled single-stranded DNA strand for signal transduction offer an alternative strategy;[28,34–37] however, such assays typically operate in a signal-off configuration[36,37] or carry a large background current in the few reported signal-on designs.[35,38] The abovementioned assay designs are prone to introducing errors in heterogeneous clinical samples that generate varying background signals.

In order to develop a reagent-free, signal-on, and low background sensor for detecting PEDv, we first discovered a PEDv-specific aptamer that we later integrated into a dual-electrode electrochemical chip (DEE-Chip). The DEE-Chip aptasensor is designed to house the aptamer bound to a DNA barcode onto one electrode and detect the released barcode on another electrode. The separation of the analyte capture and signal reporting on two different electrodes enables signal-on sensing with almost no redox background. Mass transport enhancement strategies, such as reduction of inter-electrode spacing and active field mediated transport, were also effectively harnessed to overcome slow kinetics, enabling the dual-electrode sensor to discriminate between healthy and diseased samples from 12 clinically derived porcine oral fluids in 60 mins without target labelling, amplification, or enrichment.

Results and Discussion

Aptamer Selection and Characterization

In order to develop the DEE-Chip aptasensor for detecting PEDv, we selected DNA aptamers specific to the nucleocapsid protein of PEDv (N-PEDv) using our previously described magnetic bead-based SELEX technique (Figure 1a).[26,39] We chose N-PEDv as the target analyte due its high degree of expression and ability to conserve large genetic regions during PEDv infection, which minimizes the extent of mutation relative to the spike (S) protein sites.[40,41]

Following ten rounds of selection with a library containing 6×10^{14} DNA molecules (see Table S1 for the sequences of the DNA library and primers used), high-throughput sequencing was conducted using the 10^{th} selection pool, consistent with a previously described protocol.[42] Many aptamers were discovered; the top 50 aptamer sequences based on their abundance in the final pool are listed in Table S2 (named according to their rank). The top five ranked aptamers (PEA1-PEA5) were selected for binding studies using a gel-based electrophoresis mobility shift assay (EMSA). The extracted K_d values (binding affinity) of these aptamers ranged from 2.3 to 26.3 nM (Table S2), values that are comparable with most reported aptamers for pathogen detection and thus validate the quality of the selected sequences for subsequent use in diagnostic assays.[43] As PEA1 yielded the highest affinity ($K_d=2.3$ nM) compared to the other four sequences, it was chosen for further investigation.

It is widely disseminated that shorter aptamers are more stable, cheaper to produce and easier to immobilize onto electrodes.[44] Considering these factors, we truncated PEA1 (containing 79 nucleotides; Figure 1b) to yield shorter variants. In total, 8 variants (named PEA1-1 to PEA1-8) were designed and tested for N-PEDv binding using EMSA (Figure S1). A close analysis of the data revealed that PEA1–3 (shortened to 54 nucleotides; Figure 1c) possessed an affinity ($K_d=2.8$ nM, Figure 1d and Figure S2) similar to that the full length PEA1, while a significant loss in affinity was observed for all other derivatives (Figure S1). This result suggests that the L1 and L2 loops in PEA1 play important roles in recognizing the protein target (Figure 1b).

In addition to affinity, we also tested the specificity of PEA1–3 by evaluating its binding to the following four proteins: bovine serum albumin (BSA), human α-thrombin (Tb), RNase H2 of *Clostridium difficile* (RNase H2) and the target N-PEDv protein (Figure 1e). BSA is commonly used as a control protein to test the aptamer specificity. Human α-thrombin, on the other hand, was chosen due to the existence of a high-affinity DNA aptamer that specifically recognizes this human protein[45] while RNase H2 was chosen to represent a nucleic acid binding protein. We did not observe any significant binding of PEA1–3 to the control proteins. We further tested aptamer-specific interactions of PEA1–3 with the spike (S) and nucleocapsid (N) proteins of SARS-Cov-2 (another virus from the coronavirus family) and did not observe any significant binding (Figure S3), further validating the specificity of the aptamer. Owing to its

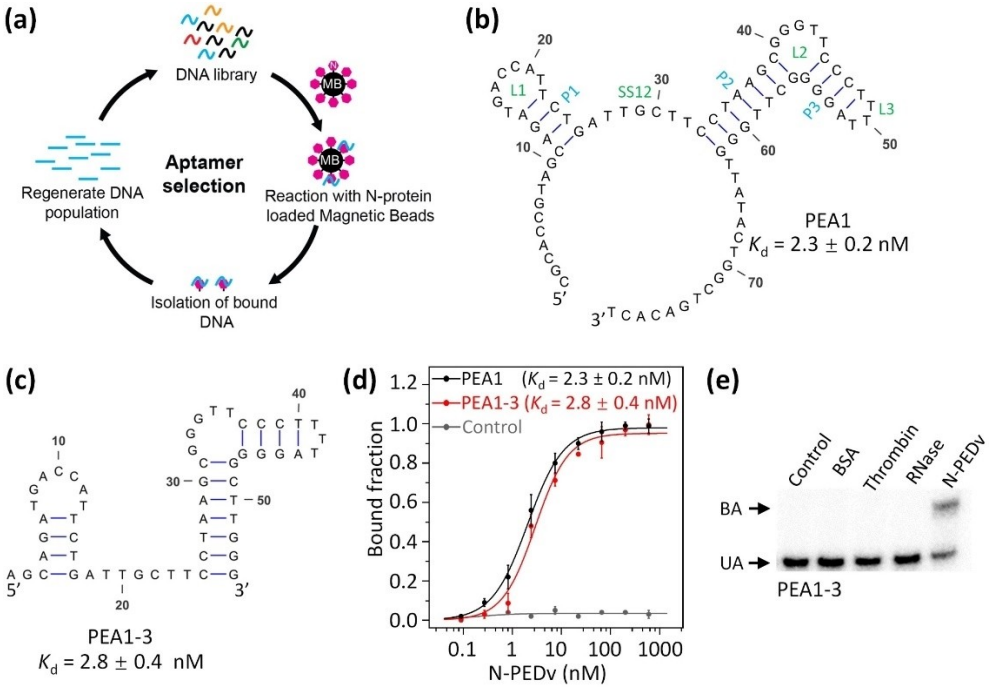

Figure 1. Aptamer selection and characterization. a) Depiction of the aptamer selection process. The secondary structures of b) full-length aptamer PEA1 and c) truncated PEA1–3. d) Binding curves and resultant affinity values (K_d, nM) extracted from the full-length and truncated aptamers binding to the nucleocapsid protein of PEDv (N-PEDv). Aptamer PEA1–3 was chosen for subsequent testing. e) Selectivity tests demonstrating PEA1–3 binding of N-PEDv (target protein) in comparison with the control proteins bovine serum albumin (BSA), thrombin, and RNase H2 of *Clostridium difficile* (RNase). A concentration of 5 nM of each protein was used in this study (BA: bound aptamer; UA: unbound aptamer).

ability to specifically identify N-PEDv, we chose PEA1–3 for constructing the reagent-less electrochemical assay for detecting PEDv.

Engineering the Dual-electrode Electrochemical Chip (DEE-Chip)

In order to integrate PEA1–3 into a reagentless electrochemical biosensor, we annealed the newly developed aptamer sequence (PEA1–3) with a methylene-blue (redox molecule) tagged bio-barcode to create an electroactive aptamer (e-aptamer), the sequence of which is given in Table S1. The e-aptamer was then integrated into *a dual-electrode electrochemical chip (DEE-Chip)* with two sensing electrodes, E_1 and E_2 (Figure 2). In this assay, E_1 is used for housing the e-aptamers on the electrochemical chip at the time of fabrication to enable reagent-less operation and for validating the chip and assay quality; whereas, E_2 is designed for generating the electrochemical signal needed for sample analysis. For constructing the DEE-Chip, we immobilized the e-aptamers onto E_1 and modified E_2 with single-stranded DNA (ssDNA) capture probes specific to the biobarcode sequence of the e-aptamer (Figure 2). In the presence of the target protein, the redox barcode is designed to be released from E_1, diffuse on the DEE-Chip, and then be recaptured on E_2 for signal generation. The two related yet separate events on E_1 and E_2 are expected to yield a signal attenuation on E_1 and signal increase on E_2 upon target capture. To facilitate the barcode release from E_1, we designed several mismatched base pairs between the aptamer PEA1–3 and barcode (Figure 2c and S4). Five barcode sequences were designed to form partial duplexes with PEA1–3 and the release of the barcode was assessed using native polyacrylamide gel electrophoresis with radiolabeled barcodes and PEA1–3 in the presences of N-PEDv protein. Barcode-3, which showed the highest release (91.2 %), was chosen as the bio-barcode for setting up the electrochemical tests (Figure S4 and Table S1).

Electrochemical chips comprised of star-shaped E_1 and E_2 gold electrodes patterned onto polystyrene substrates were fabricated for small volume (10 µL) bioanalysis. Electrodeposition of gold was then employed to derive the three-dimensional nanostructured architecture required for sensitive detection at both electrodes[46,47] (Figure S5). Diffusion-limited growth stemming from the presence of sharp edges along the star electrodes served as the main driving force in generating this dense nanostructured topography.[48,49] To ensure successful reproducibility and function of the devised platform, 1) extensive electrochemical cleaning of the electrodes was conducted prior to e-aptamer and probe bio-functionalization, 2) reproducible electroactive surface area generation was conducted on both E_1 and E_2 using cyclic voltammetry in sulfuric acid (Figure S6a), and 3) sufficient e-aptamer and probe bio-functionalization was verified for E_1 and E_2 using cyclic-voltammetry measurements in 2 mM $K_4Fe(CN)_6$ (Figure S6b). Electrodes that significantly deviated from the

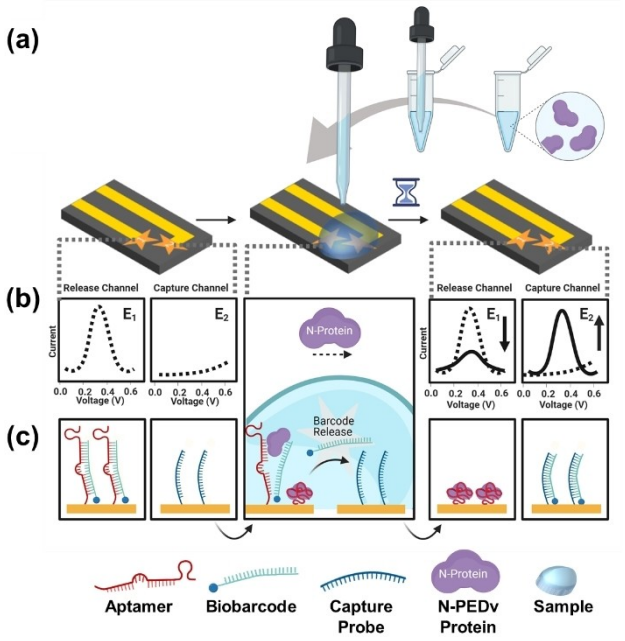

Figure 2. Schematic illustration of the operating principles and the components of the DEE-Chip assay. a) Sample-to-test workflow: liquid samples comprising of N-PEDv are introduced to the DEE-Chip using a dropper. b) Signal changes: Left: Prior to sample introduction, a methylene blue redox peak is exhibited by E_1 while an absence of this peak is exhibited on E_2. Right: Following N-PEDv introduction, target induced displacement of the redox barcode on E_1 and subsequent capture on E_2 yields a decrease in the methylene blue peak on E_1 while a signal increase is seen on E_2. c) Molecular Operation: Left: E-aptamers comprised of redox barcodes are immobilized on E_1 while single-stranded DNA (ssDNA) capture probes are anchored on E_2. Middle: In the presence of the target protein (N-PEDv), these redox barcodes are released from E_1 and diffuse towards E_2. Right: Following diffusion, the redox barcodes are subsequently captured on E_2, yielding a decrease in the redox peak on E_1 and a signal increase on E_2.

expected electroactive surface area and those that did not present the expected redox signature and peak values were not used for further experiments to reduce chip and manufacturing related variabilities.

We have evaluated the storage stability of our DNA functionalized chips in a previous study.[50] Vacuum-packed chips stored at 4 °C demonstrated a 20 % decrease in signal after 30 days, which is in agreement with reported literature on storage stability of similarly functionalized gold electrodes.[51] The high signal-to-background ratio of our assay is expected to enable our assays to be usable despite the signal loss; however, the use of preservation chemistries[52] might be required in the future to overcome aging effects.

Electrochemical Assessment Against Viral Protein Load

Given its importance to the farming industry and the lack of rapid tests currently available, we chose PEDv as our clinical target. However, this assay design can be easily adapted to other viral and non-viral targets by modifying the e-aptamer to one specific to the newly chosen analyte.[53–58]

Aiming to assess the performance of the DEE-Chip in detecting clinically relevant amounts of viral protein, we first challenged the platform with known concentrations of N-PEDv spiked in buffer. Measured current changes at both E_1 and E_2 (using square wave voltammetry, SWV), were used to probe the DEE-Chip response to viral protein loads of 10 nM (0.6 $\mu g\,mL^{-1}$) to 500 nM (29 $\mu g\,mL^{-1}$) following an incubation period of 45 mins and a small sample volume of 10 µL (Figure 3a). The redox currents on each electrode were generated through the electrochemical reduction of methylene blue that was tagged on the DNA barcode. The ensuing signal-changes were quantified by measuring the redox current before (baseline; $I\,E_{1\,before}$, $I\,E_{2\,before}$) and after (signal; $I\,E_{1\,after}$, $I\,E_{2\,after}$) viral protein loading of the DEE-Chip, with the resultant signal-changes [*Signal Change E* ($\Delta I\,E/I\,E$) $= (I\,E_{\,after} - I\,E_{\,before}) \div I\,E_{\,before}$)] then extracted to yield the sensor response calibration curve (Figure 3b). Prior to target introduction, e-aptamers immobilized on E_1 bring methylene blue moieties close to the gold surface. As this electrode is stepped through a series of potential pulses, reduction of methylene blue at the electrode gives rise to a characteristic voltametric peak at −0.3 V (baseline; Figure 3b (left, inset)).[59] Concurrently, an absence of this redox signature is observed on E_2 due to the lack of methylene blue (baseline; Figure 3b (right, inset)). In this manner, a device comprising of a signal-off (E_1) electrode and a signal-on electrode (E_2) is designed on a single chip, in which both electrodes are operated under identical experimental conditions.

As anticipated, we observed opposing trends in signal-changes on E_1 and E_2 that monotonically decreased (Figure 3b, left)) and increased (Figure 3b, right) with target concentration, respectively. It is interesting to note that a signal saturation is exhibited at both electrodes at a target concentration of 500 nM (29 $\mu g\,mL^{-1}$), likely due to the saturation of available capture sites on E_1 and E_2. A regression fit to the linear region of the calibration curve yielded a limit-of-detection (LOD) of 14 nM (0.82 $\mu g\,mL^{-1}$; 8.2 ng for a sample volume of 10 µL/electrode) for the signal-off electrode, whereas a LOD of 10 nM (0.60 $\mu g\,mL^{-1}$; 6.0 ng) was exhibited by the signal-on electrode in buffer (Figure 3b).

To evaluate the effectiveness of the DEE-Chip in working in relevant matrices, we spiked the viral protein targets (10 µL sample volume) in 30 % swine saliva. However, in order to compensate for the increased non-specific adsorption in this biological matrix, thiol terminated polyethylene glycol (PEG) was used as the anti-fouling agent. Furthermore, the incubation period was increased from 45 mins to 120 mins to account for the increased diffusion time required by the bio-barcode within the more viscous saliva matrix.[60] Trends mirroring those demonstrated in the buffer-spiked study were seen in SWV curves obtained using saliva-spiked samples (Figure 3c). The signal-change extracted from the voltammetry curves revealed that while both the buffer and saliva study were able to distinguish between samples with and without PEDv on E_1, starting at a concentration of

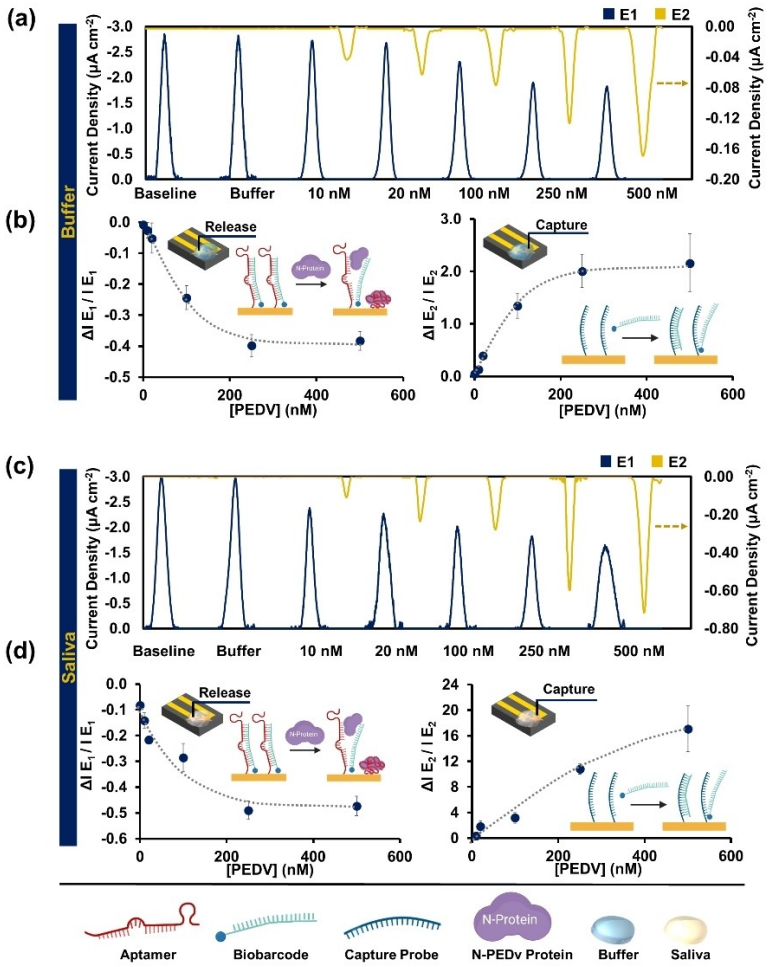

Figure 3. Dual electrode electrochemical assay for detecting PEDv nucleocapsid protein. Square wave voltammetry (SWV) curves obtained from E_1 and E_2 following incubation with various concentrations of target protein spiked in buffer (a) or 30% swine saliva (c) and incubated on the electrode for 45 mins or 120 mins, respectively. b) Calibration plots depicting the associated signal-changes in signals attained on E_1 and E_2 following incubation with target concentration of 10 nM (0.6 $\mu g\,mL^{-1}$), 20 nM (1.2 $\mu g\,mL^{-1}$),100 nM (5.8 $\mu g\,mL^{-1}$), 250 nM (14.5 $\mu g\,mL^{-1}$) and 500 nM (29.0 $\mu g\,mL^{-1}$) in buffer (b) or 30% swine saliva (d). All electrochemical measurements were performed in a 25 mM phosphate buffer solution containing 25 mM NaCl (25/25 buffer) against a silver/ silver chloride (Ag/AgCl) reference electrode and a platinum (Pt) counter electrode in a potential range of 0–0.45 V and a scan rate of 0.1 $V\,s^{-1}$. Error bars depict the standard deviation from the mean obtained using three ($n=3$) separate devices per sample.

10 nM (0.6 $\mu g\,mL^{-1}$), the signal-change was considerably higher in the saliva study (Figure 3d). This is largely attributed to the increased incubation time used in the saliva-spiked study. Even though signal saturation on E_2 was observed in buffer starting at a concentration of 250 nM (Figure 3b), this was not observed when saliva samples were used (Figure 3d). We attribute this to the increased viscosity of saliva and slower diffusion of barcode from E_1 to E_2 as well as non-specific binding between released barcodes and saliva components, all of which could reduce the amount of barcode available at E_2. The associated calibration curve, pertaining to the signal-changes at E_1 and E_2, revealed a LOD of 15 nM (0.89 $\mu g\,mL^{-1}$; 8.9 ng) for E_1 and a LOD of 8 nM (0.46 $\mu g\,mL^{-1}$; 4.6 ng) for E_2 in saliva (Figure 3d). Despite minute differences in LOD between buffer spiked and saliva spiked samples, both samples yielded LODs that fall well within the clinically relevant range reported. More specifically, considering the 10 uL analysis volume, the method is capable of detecting as low as 4.6 ng of the protein in saliva, which is in line with the reported values of 440 ng on day 3 or 66.3 ng on day 7 in rectal swabs.[61] This is further bolstered by the finding that a significantly higher magnitude of shedding is observed in oral fluids as compared to rectal swabs during the 14 days post-infection with PEDv.[62] The large signal-changes achieved on E_2 and the resultant LOD are facilitated by our unique two-electrode design that suppresses background contributions on E_2.[63] Rapid antigen tests often require sample dilution to both reduce non-specific binding and control sample viscosity.[64] We examined whether this is necessary for our newly developed assay (Figure S7). Our data demonstrate that despite the observed signal change on E_1 in the presence of N-PEDv in undiluted saliva, negligible signals are generated on E_2. However, the signal on E_2 is recovered when saliva is diluted to 30%. The

lack of signal on E_2 in undiluted saliva is likely related to the reduced mass transport from E_1 to E_2 due to the high viscosity of undiluted saliva, non-specific binding between saliva components and the barcode, and the non-specific binding of saliva components with the probe on E_2, all of which could have affected the signal generation at E_2.

Specificity of the DEE-Chip Assay

To further explore the integrity of the devised platform, we investigated whether the DEE-Chip assay could specifically recognize N-PEDv targets. We challenged the sensor by introducing a panel of non-target proteins including thrombin, bovine serum albumin (BSA), and ribonuclease (RNase) spiked in 30% healthy porcine saliva. The DEE-Chip displayed remarkable specificity, accurately distinguishing the N-PEDv samples from the nonspecific panel on both E_1 and E_2 (Figure 4a–c). Moreover, a significantly high signal-change of 10.80 was observed on E_2 when it was incubated with the N-PED sample compared to relatively insignificant signal-changes of 0.00, 0.09 and 0.41 for thrombin, BSA and RNase respectively, demonstrating the exceptional specificity of the assay. The use of two separate, yet related biorecognition events—target binding on E_1 and barcode binding and signal transduction on E_2—reduces the effect of nonspecific binding occurring on E_1 on the signal generated on E_2, contributing to the high specificity of this assay.

Kinetics Analysis and Optimization

While the engineered DEE-Chip embodies the analytical sensitivity and specificity required for N-PED detection in saliva, a detection period of 120 mins is undesirable for on-farm testing. To overcome this limitation, we explored whether strategies such as reduction of inter-electrode distance and electric field-mediated barcode transport could be leveraged to accelerate mass transport and reduce the required incubation times.[65] Towards this end, we examined the kinetics of the sensor response by measuring the signal-changes on the two electrodes as a function of incubation time (Figure 5) for three different electrode configurations (Figure 5a). The first configuration represents the original assay design, with an inter-electrode spacing "x" of 500 µm between E_1 and E_2 (Figure 5a,i). This was used to probe and identify the limitations inherent to our original design (as used in Figure 3). The second configuration features a reduced inter-electrode spacing "y" of 300 µm between the two electrodes (Figure 5a,ii), allowing us to directly probe whether decreasing the inter-electrode distance is sufficient to overcome the challenge of transporting the barcode through the viscous salivary medium to E_2 in under 120 mins. The last configuration explores the use of a positive bias potential, applied on E_2, in conjunction with an interelectrode spacing of 300 µm (Figure 5a,iii) to drive the negatively charged DNA barcode via electro-migration from E_1 to E_2.

Plots representing the release and capture kinetics observed in each of these three cases reveal that on E_1, a linear decrease in signal-change is observed between 15 and 60 mins, with the slope of the curve decreasing after 60 mins

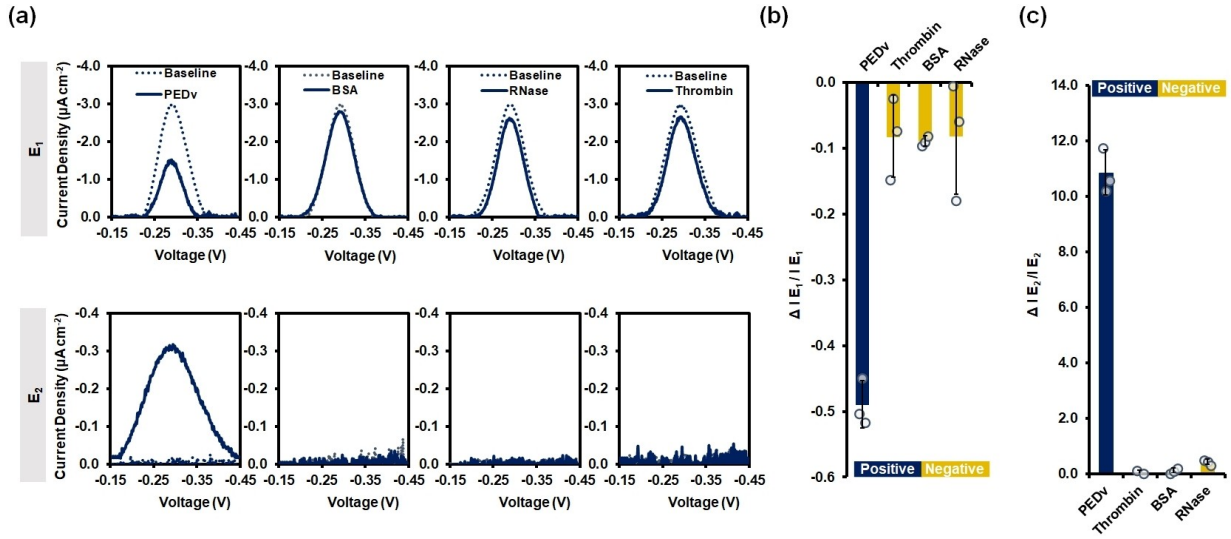

Figure 4. Specificity testing of the DEE-Chip in 30% porcine saliva. a) Square wave voltammograms representing the signal-changes obtained from a pair of E_1 and E_2 electrodes. Each pair was separately incubated with 250 nM N-PEDv (target protein), bovine serum albumin (BSA), thrombin and ribonuclease (RNase) spiked in 30% porcine saliva. Jitter-plots comparing the signal responses obtained from E_1 (b) and E_2 (c) in the presence of target (N-PEDv) and control (thrombin, BSA, RNase) proteins. All electrochemical measurements were performed in a 25 mM phosphate buffer solution containing 25 mM NaCl (25/25 buffer) against a silver/ silver chloride (Ag/AgCl) electrode and a platinum (Pt) counter electrode in a potential range of 0–0.45 V and a scan rate of 0.1 $V s^{-1}$. Error bars depict the standard deviation from the mean obtained using three ($n=3$) separate devices per sample.

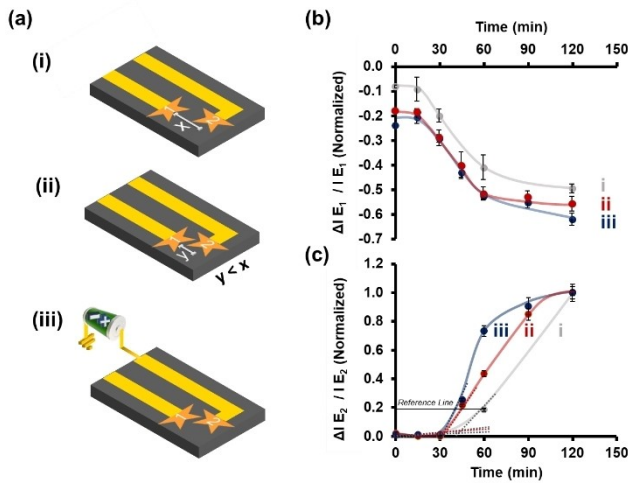

Figure 5. Developing engineering strategies for reducing assay time. a) A visual representation of the engineering changes made to the DEE-Chip for reducing assay time. The first case (i) demonstrates the original inter-electrode spacing "$x = 500$ µm" between E_1 and E_2. Scenario (ii) depicts the reduction of this inter-electrode spacing to "$y = 300$ µm". Scenario (iii) portrays the use of inter-electrode spacing "y" in conjunction with an applied positive potential bias (+0.5 V) on E_2. b), c) Plots represent the release and capture kinetics observed in each of the three cases depicted in (a). Dotted lines in (c) indicate signal onset; extracted using tangents constructed to linearly extrapolate signal response at the first true-signal (non-noise) data points and at the data point prior to the first true-signal (non-noise) data (indicated by reference lines). For each group, $n = 3$ independent devices were tested per sample, each incubated with 500 nM of N-PEDv at a sample volume of 10 µL. The data are presented as mean ± standard deviation with visual guidelines depicting the overall trend in each scenario.

(Figure 5b). Redox-tagged barcodes are increasingly released between 15 and 60 mins as target proteins bind to the surface immobilized e-aptamers. A plateau in signal-change is subsequently attained at 120 mins as accessible e-aptamer sites on E_1 are exhausted. In case "i" ($x = 500$ µm), capture of the released barcodes begins at 43 mins, rising exponentially until a capture of >50 % is attained by 120 mins (Figure 5c,i). Using a diffusion coefficient (D) of $\approx 1.18 \times 10^{-10}$ $m^2 s^{-1}$, as deduced from a fluorescein-tagged 33-nucleotide oligomer navigating an aqueous solution,[66] we calculate that it takes 17.7 mins ($\tau = x^2/2D$) for the barcode to diffuse through an inter-electrode distance (x) of 500 µm. Given that the signal onset (43 mins) takes longer than the diffusion time (estimated ≈18 mins in aqueous media), we hypothesize that the viscosity of the salivary matrix lowers the reaction kinetics. Reducing the inter-electrode distance to 300 µm to overcome this inherent diffusion time barrier causes the theoretical diffusion time to reduce to 6.4 mins, which correlates to a practical observed signal onset at 33 mins (Figure 5c, ii). Inspired by the electrophoretic motion of DNA fragments through gels, we applied a positive potential bias across E_2 to further aid in diffusion of the barcode through saliva. Time-resolved electrochemical measurements revealed that while signal onset mirrored that of detection without the application of a bias-potential (case ii), the signal-change increased at a much faster rate between 30 and 60 mins, reaching 75 % of its final value at 60 minutes compared to much lower values for the first (20 %) and second (45 %) configurations (Figure 5c, iii). The improved signal detection achieved for sensors employing both the reduction of inter-electrode distance and the application of a bias potential supports the reduction of detection time from 120 mins (case i; *original design*) to 60 mins (*optimized design*) for facilitating rapid on-farm analysis. We have also measured the specificity and limit-of-detection of the DEE-Chips with a reduced inter-electrode distance and under an applied bias (scenario (iii)). As expected, the redesigned chips enhanced the limit-of-detection measured on E2 (6 nM in saliva and in 60 minutes). Additionally, the chip redesign did not affect the assay specificity (Figure S8).

Clinical Detection

Given the literature evidence supporting the presence of sufficient viral loads in the oral fluid samples for up to 35 days post-infection as measured by reverse transcription PCR (RT-PCR), we expected viral detection in saliva to be feasible using our assay.[62] We next assessed the capability of the DEE-Chip for detecting PEDv in clinical swine saliva samples. We analyzed 12 anonymized, clinically-sourced swine oral fluid samples (Figure 6), six of which were established as PEDv-positive and 6 of which were determined to be PEDv-negative by RT-PCR (Figure S9). Following lysis and dilution, the porcine saliva samples were analyzed using DEE-Chips for 60 mins (Figure 6a).

PEDv-positive samples exhibited a larger signal change (0.44–0.75) compared to PEDv-negative samples (0.05–0.30) on E_1 (Figure 6b). This was paralleled by much larger signal differences observed between positive (3.0–20.8) and negatives samples (<0.90) on E_2 (Figure 6c). It is important to note that the DEE-Chip was unable to identify the presence of PEDv in positive sample 4. In addition, small variations in the magnitude of signal-change were observed with the different samples, which is likely due to the differences in the composition of the individual saliva samples and their respective viral loads. Despite these variations, the electrochemical assay retains its performance over a range of statistically significant cycle threshold (C_t) values derived from PCR (i.e., C_t of 28.9–28.6 for positive samples 1–3 and C_t of 33.2–33.1 for positive samples 5–6). It should be noted that the false-negative sample 4 had the largest C_t value (33.9) amongst the samples and as such the lowest viral load. There are two hypotheses for the rationale behind the false-negative result generated using sample 4: 1) an insufficient viral load and 2) the presence of salivary inhibitory factors that prevent bio-recognition by the aptamer on E_1. We tested these two hypotheses by re-analyzing the false-negative sample and manually spiking it with PEDv at a concentration of 500 nM (Figure S10). The signal-changes elicited were then compared against an unspiked false-negative analogue and a PEDv negative sample. Of these, only the PEDv spiked samples exhibited a significant signal-

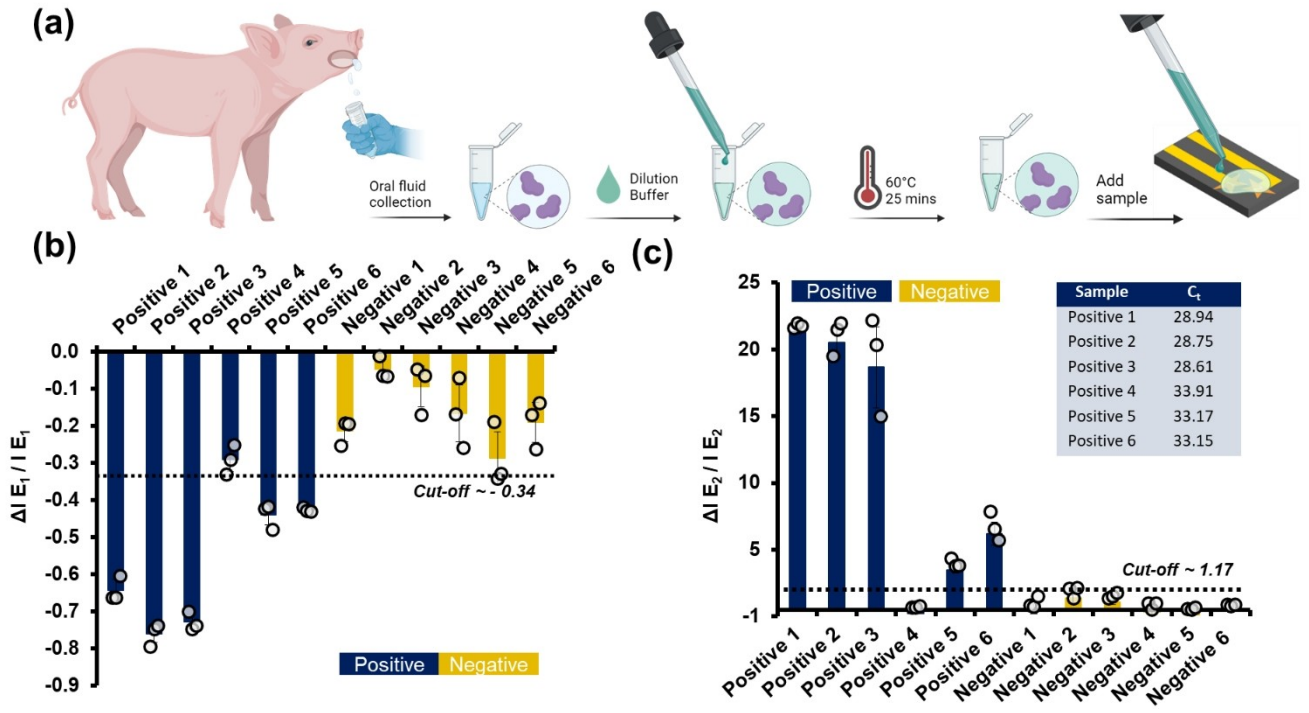

Figure 6. Clinical evaluation of the DEE-Chip. a) Illustration of the diagnostic workflow from sample collection to sensor operation. Following sample dilution and heating, the collected porcine saliva sample is added to the DEE-Chip, incubated for 60 mins at room temperature and scanned using a portable potentiostat. Jitter-plots depicting signal-changes measured on b) E_1 and c) E_2 for six clinically-obtained PEDv positive (navy) and six negative (yellow) porcine saliva samples. Dotted lines indicate the cut-off threshold of the assay as extracted using the "Analyse-it" toolkit in excel. The bars represent the mean of the signal-change extracted from square wave voltammograms on E_1 and E_2 for a given sample. The error bars represent the standard deviation from the mean obtained using three ($n=3$) separate devices per sample. All square wave voltammograms were obtained using 25 mM phosphate buffer solution containing 25 mM NaCl (25/25 buffer) as the supporting electrolyte against a silver / silver chloride (Ag/AgCl) electrode and a platinum (Pt) counter electrode in a potential range of 0–0.45 V and a scan rate of 0.1 $V s^{-1}$. In addition, E_2 electrodes were biased using a bias potential of +0.5 V to reduce the detection window to 60 mins.

change (0.53) on E_1 and a large gain in signal-change (17.83) on E_2. The ability of the DEE-Chip to detect the spiked sample rules out salivary inhibitory factors, pointing to the insufficient viral load as the reason for the negative response (consistent with the high C_t value of sample 4).

Receiver Operator Characteristics (ROC) curves constructed from the data from the DEE-Chip (Figure 6b,c) were subsequently used to assess the clinical performance of this assay (Figure S11).[24,67] An overall accuracy, or area under the curve (AUC), of 0.975 (CI, 0.936–1.014), sensitivity of 83 %, and specificity of 100 % were obtained at a decision threshold of −0.34 (signal-change) on E_1. A corresponding AUC of 0.873 (CI, 0.735–1.012), sensitivity of 83 %, and specificity of 100 %, at a threshold of 1.16 (signal-change) were obtained using E_2 data. We have also used our calibration curve (Figure S8a) to convert the electrochemical metrics to analytical metrics (Figure S12). The signal ranges for the positive samples on E_2 ranged from 12–613 nM (0.68–27 $\mu g mL^{-1}$ (Figure S12)). Inspection of the clinical performance metrics (sensitivity, specificity and AUC) reveals that the DEE-Chip performance falls well within the standard threshold of a reliable diagnostic test (AUC >0.8,[68] sensitivity $\geq 80\,\%$[69] and specificity $\geq 90\,\%$[69]), thereby indicating the potential of this assay for future clinical use.

Conclusion

Considering recurrent surges in PEDv outbreaks coupled with increasing reports of emerging viral pathogens in animals, the need for a simple, on-farm, saliva-based viral test is more critical than ever. In response, we developed a rapid, simple, and reagent-less assay for on-farm detection of PEDv. We developed a dual-electrode electrochemical Chip (DEE-Chip) featuring functional e-aptamers for PEDv testing. Towards this end, SELEX was first employed to select a novel high-affinity DNA aptamer ($K_d = 2.3$ nM) that discriminately targets the highly conserved and mutation-resistant N-protein of the PEDv virus. The DEE-Chip uses a unique approach for integrating the PEDv aptamer for reagent-less sensing; it includes one electrode for housing the aptamer annealed with a redox DNA barcode and another electrode for capturing the DNA barcode and transducing an electrochemical signal. Using this approach, the DEE-Chip yielded clinically relevant LODs of 14 nM (0.82 $\mu g mL^{-1}$; E_1) and 10 nM (0.60 $\mu g mL^{-1}$; E_1) in 10 µL of

buffer-spiked N-PEDv samples; while clinically relevant LODs of 15 nM (0.89 $\mu g\,mL^{-1}$; E_1) and 8 nM (0.46 $\mu g\,mL^{-1}$; E_2) were obtained using saliva-spiked N-PEDv samples.

To reduce the assay time (initially 120 mins) for rapid on-farm testing, we focused on engineering the inter-electrode spacing of the chip and the use of a bias potential to enhance the mass transport of the DNA barcode from one electrode to another. Using the re-engineered DEE-Chip, we analyzed 12 clinically-derived swine saliva samples. The DEE-Chip successfully analyzed 92 % (and 100 % of all samples for $C_t \leq 33.17$) of the clinical samples with a clinical sensitivity of 83 %, specificity of 100 % and LOD of 6 nM (0.37 $\mu g\,mL^{-1}$; E_2) in 60 mins without target amplification, target enrichment, target labelling, or the addition of read-out reagents. The DEE-Chip is versatile and can be integrated with other e-aptamers for detecting various bioanalytes, including other viruses and bacteria, for fulfilling the unmet need of rapid and on-farm animal disease surveillance.

Experimental Section

Comprehensive experimental procedures were placed in the Supporting Information.

Acknowledgements

The work is supported by the Natural Science and Engineering Research Council (NSERC) of Canada. L.S. is supported by the Canada Research Chair program. The electron microscopy was carried out at the Canadian Centre for Electron Microscopy (CCEM), a national facility supported by the NSERC and McMaster University. In-kind collection, PCR diagnostic testing and provision of all farm samples was carried out by South West Ontario Veterinary Services, Stratford, Ontario.

Conflict of Interest

The authors declare no conflict of interest.

Keywords: Animal Testing · Aptamers · Coronavirus · Electrochemical Biosensors · Porcine Epidemic Diarrhea Viruses

[1] J. Cui, F. Li, Z.-L. Shi, *Nat. Rev. Microbiol.* **2019**, *17*, 181–192.
[2] S. N. Bevins, M. Lutman, K. Pedersen, N. Barrett, T. Gidlewski, T. J. Deliberto, A. B. Franklin, *Emerging Infect. Dis.* **2018**, *24*, 1390–1392.
[3] L. L. Schulz, G. T. Tonsor, *J. Anim. Sci.* **2015**, *93*, 5111–5118.
[4] A. Bang, S. Khadakkar, *Proc. Natl. Acad. Sci. USA* **2020**, *117*, 29995–29999.
[5] S. Chen, L. Zhang, L. Wang, H. Ouyang, L. Ren, *Proc. Natl. Acad. Sci. USA* **2021**, *118*, e2022344118.
[6] J. Vidic, M. Manzano, C.-M. Chang, N. Jaffrezic-Renault, *Vet. Res.* **2017**, *48*, 11.
[7] A. Cullinane, M. Garvey, *Rev. Sci. Tech.* **2021**, *40*, 75–89.
[8] S. Neethirajan, S. K. Tuteja, S.-T. Huang, D. Kelton, *Biosens. Bioelectron.* **2017**, *98*, 398–407.
[9] A. Kang, M. Yeom, H. Kim, S.-W. Yoon, D.-G. Jeong, H.-J. Moon, K.-S. Lyoo, W. Na, D. Song, *Immune Netw.* **2021**, *21*, e11.
[10] S. Zou, L. Wu, G. Li, J. Wang, D. Cao, T. Xu, A. Jia, Y. Tang, *Anim. Dis.* **2021**, *1*, 27.
[11] W. Xiao, C. Huang, F. Xu, J. Yan, H. Bian, Q. Fu, K. Xie, L. Wang, Y. Tang, *Sens. Actuators B* **2018**, *266*, 63–70.
[12] B. Fan, J. Sun, L. Zhu, J. Zhou, Y. Zhao, Z. Yu, B. Sun, R. Guo, K. He, B. Li, *Front. Vet. Sci.* **2020**, *7*, 540248.
[13] K. Poonsuk, T.-Y. Cheng, J. Ji, J. Zimmerman, L. Giménez-Lirola, *Porc. Health Manag.* **2018**, *4*, 31.
[14] I. Díaz, J. Pujols, E. Cano, R. Cuadrado, N. Navarro, E. Mateu, M. Martín, *Vet. Immunol. Immunopathol.* **2021**, *234*, 110206.
[15] J. S. Oh, D. S. Song, J. S. Yang, J. Y. Song, H. J. Moon, T. Y. Kim, B. K. Park, *J. Vet. Sci.* **2005**, *6*, 349–352.
[16] Z. Ma, T. Wang, Z. Li, X. Guo, Y. Tian, Y. Li, S. Xiao, *J. Nanobiotechnol.* **2019**, *17*, 96.
[17] W.-T. Hsu, C.-Y. Chang, C.-H. Tsai, S.-C. Wei, H.-R. Lo, R. J. S. Lamis, H.-W. Chang, Y.-C. Chao, *Viruses* **2021**, *13*, 303.
[18] J. Ma, L. Wu, Z. Li, Z. Lu, W. Yin, A. Nie, F. Ding, B. Wang, H. Han, *Anal. Chem.* **2018**, *90*, 7415–7421.
[19] J. Ma, W. Wang, Y. Li, Z. Lu, X. Tan, H. Han, *Anal. Chem.* **2021**, *93*, 2090–2096.
[20] X. Li, Y. Wang, X. Zhang, Y. Gao, C. Sun, Y. Ding, F. Feng, W. Jin, G. Yang, *Microchim. Acta* **2020**, *187*, 217.
[21] E. M. McConnell, I. Cozma, D. Morrison, Y. Li, *Anal. Chem.* **2020**, *92*, 327–344.
[22] M. N. Kammer, A. Kussrow, I. Gandhi, R. Drabek, R. H. Batchelor, G. W. Jackson, D. J. Bornhop, *Anal. Chem.* **2019**, *91*, 10582–10588.
[23] J. S. Swensen, Y. Xiao, B. S. Ferguson, A. A. Lubin, R. Y. Lai, A. J. Heeger, K. W. Plaxco, H. Tom Soh, *J. Am. Chem. Soc.* **2009**, *131*, 4262–4266.
[24] Z. Zhang, R. Pandey, J. Li, J. Gu, D. White, H. D. Stacey, J. C. Ang, C. Steinberg, A. Capretta, C. D. M. Filipe, K. Mossman, C. Balion, M. S. Miller, B. J. Salena, D. Yamamura, L. Soleymani, J. D. Brennan, Y. Li, *Angew. Chem. Int. Ed.* **2021**, *60*, 24266–24274; *Angew. Chem.* **2021**, *133*, 24468–24476.
[25] Z. Zhang, J. Li, J. Gu, R. Amini, H. D. Stacey, J. C. Ang, D. White, C. D. M. Filipe, K. Mossman, M. S. Miller, B. J. Salena, D. Yamamura, P. Sen, L. Soleymani, J. D. Brennan, Y. Li, *Chem. Eur. J.* **2022**, *28*, e202200078.
[26] J. Li, Z. Zhang, J. Gu, H. D. Stacey, J. C. Ang, A. Capretta, C. D. M. Filipe, K. L. Mossman, C. Balion, B. J. Salena, D. Yamamura, L. Soleymani, M. S. Miller, J. D. Brennan, Y. Li, *Nucleic Acids Res.* **2021**, *49*, 7267–7279.
[27] D. Song, B. Park, *Virus Genes* **2012**, *44*, 167–175.
[28] T. A. Feagin, N. Maganzini, H. T. Soh, *ACS Sens.* **2018**, *3*, 1611–1615.
[29] L. R. Schoukroun-Barnes, F. C. Macazo, B. Gutierrez, J. Lottermoser, J. Liu, R. J. White, *Annu. Rev. Anal. Chem.* **2016**, *9*, 163–181.
[30] R. J. White, A. A. Rowe, K. W. Plaxco, *Analyst* **2010**, *135*, 589–594.
[31] Y. Xiao, T. Uzawa, R. J. White, D. DeMartini, K. W. Plaxco, *Electroanalysis* **2009**, *21*, 1267–1271.
[32] Y. Xiao, A. A. Lubin, A. J. Heeger, K. W. Plaxco, *Angew. Chem. Int. Ed.* **2005**, *44*, 5456–5459; *Angew. Chem.* **2005**, *117*, 5592–5595.
[33] D.-Y. Liu, Y. Zhao, X.-W. He, X.-B. Yin, *Biosens. Bioelectron.* **2011**, *26*, 2905–2910.
[34] Z. Tang, P. Mallikaratchy, R. Yang, Y. Kim, Z. Zhu, H. Wang, W. Tan, *J. Am. Chem. Soc.* **2008**, *130*, 11268–11269.

[35] Y. Xiao, B. D. Piorek, K. W. Plaxco, A. J. Heeger, *J. Am. Chem. Soc.* **2005**, *127*, 17990–17991.
[36] R. Liu, Z. Yang, Q. Guo, J. Zhao, J. Ma, Q. Kang, Y. Tang, Y. Xue, X. Lou, M. He, *Electrochim. Acta* **2015**, *182*, 516–523.
[37] K. Feng, C. Sun, Y. Kang, J. Chen, J.-H. Jiang, G.-L. Shen, R.-Q. Yu, *Electrochem. Commun.* **2008**, *10*, 531–535.
[38] Y. Xiao, X. Qu, K. W. Plaxco, A. J. Heeger, *J. Am. Chem. Soc.* **2007**, *129*, 11896–11897.
[39] M. Liu, J. Wang, Y. Chang, Q. Zhang, D. Chang, C. Y. Hui, J. D. Brennan, Y. Li, *Angew. Chem. Int. Ed.* **2020**, *59*, 7706–7710; *Angew. Chem.* **2020**, *132*, 7780–7784.
[40] B. Liwnaree, J. Narkpuk, S. Sungsuwan, A. Jongkaewwattana, P. Jaru-Ampornpan, *PLoS One* **2019**, *14*, e0212632.
[41] F. Deng, G. Ye, Q. Liu, M. T. Navid, X. Zhong, Y. Li, C. Wan, S. Xiao, Q. He, Z. F. Fu, G. Peng, *Viruses* **2016**, *8*, 55.
[42] R. Gysbers, K. Tram, J. Gu, Y. Li, *Sci. Rep.* **2015**, *5*, 11405.
[43] D. Chang, S. Zakaria, S. Esmaeili Samani, Y. Chang, C. D. Filipe, L. Soleymani, J. D. Brennan, M. Liu, Y. Li, *Acc. Chem. Res.* **2021**, *54*, 3540–3549.
[44] M. Elbadawi, J. J. Ong, T. D. Pollard, S. Gaisford, A. W. Basit, *Adv. Funct. Mater.* **2021**, *31*, 2006407.
[45] I. Russo Krauss, A. Merlino, A. Randazzo, E. Novellino, L. Mazzarella, F. Sica, *Nucleic Acids Res.* **2012**, *40*, 8119–8128.
[46] L. Soleymani, Z. Fang, E. H. Sargent, S. O. Kelley, *Nat. Nanotechnol.* **2009**, *4*, 844–848.
[47] L. Soleymani, Z. Fang, X. Sun, H. Yang, B. J. Taft, E. H. Sargent, S. O. Kelley, *Angew. Chem. Int. Ed.* **2009**, *48*, 8457–8460; *Angew. Chem.* **2009**, *121*, 8609–8612.
[48] G. Rabai, M. Orban, I. R. Epstein, *Acc. Chem. Res.* **1990**, *23*, 258–263.
[49] S. M. Traynor, G. A. Wang, R. Pandey, F. Li, L. Soleymani, *Angew. Chem. Int. Ed.* **2020**, *59*, 22617–22622; *Angew. Chem.* **2020**, *132*, 22806–22811.
[50] R. Pandey, Y. Lu, E. Osman, S. Saxena, Z. Zhang, S. Qian, A. Pollinzi, M. Smieja, Y. Li, L. Soleymani, T. Hoare, *ACS Sens.* **2022**, *7*, 985–994.
[51] F. Kuralay, S. Campuzano, J. Wang, *Talanta* **2012**, *99*, 155–160.
[52] P. Wu, D. W. Grainger, *J. Proteome Res.* **2006**, *5*, 2956–2965.
[53] Z. Chen, Q. Wu, J. Chen, X. Ni, J. Dai, *Virol. Sin.* **2020**, *35*, 351–354.
[54] R. Wang, J. Zhao, T. Jiang, Y. M. Kwon, H. Lu, P. Jiao, M. Liao, Y. Li, *J. Virol. Methods* **2013**, *189*, 362–369.
[55] K. Percze, Z. Szakács, É. Scholz, J. András, Z. Szeitner, C. H. Kieboom, G. Ferwerda, M. I. de Jonge, R. E. Gyurcsányi, T. Mészáros, *Sci. Rep.* **2017**, *7*, 42794.
[56] X. Zou, J. Wu, J. Gu, L. Shen, L. Mao, *Front. Microbiol.* **2019**, *10*, 1462.
[57] S. Dolai, M. Tabib-Azar, *Med. Devices Sens.* **2020**, *3*, e10112.
[58] J. Kang, G. Yeom, S.-J. Ha, M.-G. Kim, *New J. Chem.* **2019**, *43*, 6883–6889.
[59] S. O. Kelley, J. K. Barton, N. M. Jackson, M. G. Hill, *Bioconjugate Chem.* **1997**, *8*, 31–37.
[60] K. Ngamchuea, C. Batchelor-McAuley, R. G. Compton, *Sens. Actuators B* **2018**, *262*, 404–410.
[61] K. L. Baker, P. R. Thomas, L. A. Karriker, A. Ramirez, J. Zhang, C. Wang, D. J. Holtkamp, *BMC Vet. Res.* **2017**, *13*, 372.
[62] J. Bjustrom-Kraft, K. Woodard, L. Giménez-Lirola, M. Rotolo, C. Wang, Y. Sun, P. Lasley, J. Zhang, D. Baum, P. Gauger, *BMC Vet. Res.* **2016**, *12*, 99.
[63] R. Pandey, D. Chang, M. Smieja, T. Hoare, Y. Li, L. Soleymani, *Nat. Chem.* **2021**, *13*, 895–901.
[64] G. C. Mak, P. K. Cheng, S. S. Lau, K. K. Wong, C. Lau, E. T. Lam, R. C. Chan, D. N. Tsang, *J. Clin. Virol.* **2020**, *129*, 104500.
[65] L. Soleymani, F. Li, *ACS Sens.* **2017**, *2*, 458–467.
[66] A. Werner, *Nucleic Acids Res.* **2011**, *39*, e17–e17.
[67] M. H. Zweig, G. Campbell, *Clin. Chem.* **1993**, *39*, 561–577.
[68] J. N. Mandrekar, *J. Thorac. Oncol.* **2010**, *5*, 1315–1316.
[69] World Health Organization, *Antigen-Detection in the Diagnosis of SARS-CoV-2 Infection: Interim Guidance*, *6 October 2021*, World Health Organization, **2021**.

Manuscript received: March 22, 2022
Accepted manuscript online: May 13, 2022
Version of record online: June 9, 2022